ChemPubSoc Europe

DOI: 10.1002/cphc.201801173

CHEMPHYSCHEM Articles

Density Functional Theory Study of Aspirin Adsorption on BCN Sheets and their Hydrogen Evolution Reaction Activity: a Comparative Study with Graphene and Hexagonal Boron Nitride**

Vivek K. Yadav,[a] Showkat H. Mir,[a] and Jayant K. Singh*[a]

We explored the aspirin adsorption and their hydrogen evolution reaction (HER) activity in waste water of borocarbonitride sheets. Our results indicate that BCN sheets considered here show HER activity and exhibit superior performance regarding adsorption of aspirin in waste water in comparison with graphene and hexagonal boron nitride (h-BN). The drug molecule (aspirin) possesses a strong affinity to BCN, with the order of binding energy on following the order BCN ~ h-BN > graphene. Upon drug adsorption, the band gap of h-BN is found to be reduced by up to 33%, whereas the bandgaps of graphene and BCN remain unaltered *that makes BCN a potential candidate for HER in waste water.*

1. Introduction

Molecular adsorption on surfaces plays an important role that is relevant to industry and in nature such as desalination, catalysis, corrosion, etc. Pharmaceutical drugs commonly used to reduce fever such as Acetylsalicylic (ASA), Acetaminophen (APAP) and Ibuprofen comprised of a single benzene ring and oxygenated side chains. These drugs are not completely metabolized inside the body and are excreted through urine or faeces and thus go to the waste-water as a biologically active substance.[1] Besides, the indiscriminate disposal of pharmaceutical waste from manufacturing process, discarding of expired or unused drugs also reach to the waste-water.[2] Though, the amount of pharmaceutically active compounds found in the waste-water are usually very low[3,4] nevertheless, in the long-term, their continuous release to the environment poses a potential threat to the terrestrial and aquatic organisms.[5] As such treatment of waste-water containing pharmaceutical drugs is a global concern. All these drugs interact with two-dimensional (2D) sheets through $\pi - \pi$ interaction mainly arising due to the presence of benzene ring. In order to study their interaction with 2D materials, we used Acetylsalicylic or aspirin (ASA) as a template model for the above-said drugs. Graphene (GRAP) which is composed of a single layer of sp^2-hybridized carbon atoms arranged in a 2D honeycomb structure shows extraordinary physiochemical properties such as high surface area, optical transparency, large mechanical strength, and electron rich π-electron system. An isoelectronic analog of graphene, hexagonal boron nitride (h-BN) also displays excellent thermal and chemical stability. Furthermore, graphene has relatively large and delocalized π-electron system which may possess binding attributes for target molecules such as drugs, amino-acids, etc. Therefore, graphene and its sister analog materials belong to a new class of fascinating nanomaterials. This material has garnered a great interest as nano-adsorbent for pollution control applications in recent years.[6,7] Since graphene is a zero band gap material, therefore doping of hetero-atoms, boron and nitrogen in GRAP generate new materials that creates a band gap at Dirac point. These newly designed materials called as borocarbonitrides (BCN) constitutes a family of exciting 2D systems that display new electronic structure properties and applications. They also exhibit better activity towards adsorption and catalytic properties.[8–11] They have also shown good field emission properties just like carbon nanotubes (CNT).[11–13]

Experimentally, Al-Khateeb et al. investigated the removal of ASA, acetaminophen and caffeine from aqueous solution using graphene-nanoplatelets.[14] The reported adsorption capacities/order of adsorption for ASA, acetaminophen and caffeine were found as 13.02, 19.72, and 18.76, respectively in units of mg/g. Recently, a first-principles study of the binding energy of ASA on CNT and carbon nitride nanotubes (CNNT) shows that ASA binds strongly to pristine CNNT than to CNT with binding energy 0.67 and 0.51 eV respectively.[15] Such higher binding energy on CNNT was ascribed to the local intrinsic dipole moments in CNNT which results in the dipole-dipole interaction between ASA molecule and CNNT. The study also reported that no practical charge transfer takes place between CNT (CNNT) and ASA. Moreover, Al-Hamdani et al.[16] studied the interaction of water with h-BN of different dimensions (zero to 2-dimensional) with benchmark accuracy. The adsorption energy for water/h-BN reported by them was in the range of -0.107 ± 0.007 eV using diffusion Monte Carlo method with lattice regularization (LRDMC).

The water-soluble pharmaceuticals traces such as ASA have been classified as emerging pollutants due to their persistence in the ecosystem. Several methodologies have been developed

[a] *Dr. V. K. Yadav, Dr. S. H. Mir, Prof. J. K. Singh*
Department of Chemical Engineering, IIT Kanpur, Kanpur, India – 208016
E-mail: jayantks@iitk.ac.in

[**] *DFT: density functional theory; BCN: borocarbonitride*

Supporting information for this article is available on the WWW under https://doi.org/10.1002/cphc.201801173

for the treatment of waste-water such as adsorption,[17–19] reverse osmosis,[20] photocatalytic oxidation and catalytic ozonation,[21,22] nano- and ultra-filtration,[23] biological processes,[24] etc. However, adsorption is one of the most promising methods to remove contaminants from the polluted water due to its simple design and low-cost. While 2D materials have shown good adsorbent properties, they can also be used as photo-catalysts, and disinfectants in water treatment.[7] Therefore, in present work, our goal is to examine the adsorption of ASA on the GRAP, BCN and h-BN sheet via ab initio approach and to investigate the HER activity of drug adsorbed BCN.

This paper is organized as follows: in Simulation methodology, we provide the details of the methods employed in the present work. In Results and discussions, we provide information on the structural and thermodynamic stability of GRAP, BCN and h-BN by calculating cohesive and formation energy. Subsequently, we present the binding strength of ASA on various 2D sheets. In order to provide further insight on the binding strength of ASA on GRAP, BCN and h-BN, the electronic band structure and projected density of states of pristine and ASA adsorbed GRAP, BCN and h-BN sheets were also examined. We then analyzed the hydrogen evolution reaction (HER) activity of BCN sheet and showed that it may be a promising candidate for photocatalysis. We concluded the paper by giving a detailed summary of the main results of the present study with future prospects of BCN sheet.

Computational Details

All calculations in this work were performed using quantum espresso simulation code.[25] DFT calculations were performed to study the structural properties and binding energy of ASA on GRAP, h-BN and BCN. Ultrasoft pseudopotentials[26] were employed to describe electron-ion interaction using Perdew-Burke-Ernzerhof[27] functional with in the framework of generalized gradient approximation (GGA).[28] The ultrasoft pseudopotentials have been generated using Rappe-Rabe-Kaxiras-Joannopoulos (RRKJ) method.[29] The Kohn-Sham wave-functions were expanded by a plane wave basis set with the kinetic energy cutoff of 50 Ry. Brillouin zone (BZ) integration was done using a uniform Monkhorst-Pack[30] k-point grid of $5\times5\times1$ for geometry optimization and $10\times10\times1$ for electronic structure calculations. We have performed benchmark calculations in order to determine the converged values for cutoff energy and K-points as can be seen in Figure SI1. Furthermore, the convergence for energy was chosen as 10^{-8} eV between two consecutive self-consistent steps. In our calculations, we used a unit cell consisting of 72 atoms in total for all structures. For the BCN sheet, we adopted two arrangements, BCN1 comprising of 80% carbon and 20% (= 8) BN pairs approximately and BCN2 containing 75% carbon and 25% (=9) BN pairs. To avoid the interaction between periodic images a large vacuum of 20 Å was employed in the direction perpendicular to the sheet. It should be noted that van der Waals (vdWs) interactions are important for binding energy calculations, therefore, in the present work, we have used dispersion (Grimme's D3-type) corrected DFT calculations (DFT-D3)[31] to study the interactions of ASA with GRAP, BCN and h-BN. In order to study the adsorption of ASA on 2D sheets, we considered two different configurations C1 (in which O-atom of ester group in ASA is away from the sheet) and C2 (in which O-atom is facing the sheet) as shown in Figure SI2. The adsorption energy E_{ad} of ASA was calculated using the following equation.

$$E_{ad} = E_{system+ASA} - (E_{system} + E_{ASA}) \quad (1)$$

where $E_{system+ASA}$ represents the total energy of ASA adsorbed GRAP, BCN or h-BN sheets, E_{system} is the total energy of bare sheet and E_{ASA} denotes the energy of ASA molecule in the gas phase.

2. Results and Discussions

2.1. Structural Properties

The optimized structure of ASA ($C_9H_8O_4$) in vacuum is shown in Figure 1(a). It consists of an ester group, aromatic ring and carboxylic acid. Four different types of 2D structures viz. as GRAP, BCN (BCN1, BCN2) and h-BN were chosen to investigate their ability to adsorb ASA. It is worth to mention here that the four structures chosen for ASA adsorption exhibit the metallic, semi-conducting and insulating electronic properties. The optimized structures of GRAP, BCN1 and h-BN are shown in Figure 1(b,c,d). For brevity, optimized structure of BCN2 is shown in Figure SI3. The C–C and B–N bond lengths calculated for GRAP and h-BN were 1.420 and 1.440 Å which are in good agreement with the theoretical results.[32,33] For BCN sheets, the calculated C–C, C–N, C–B and B–N bond lengths were 1.423, 1.376, 1.476 and 1.455 Å. It is seen that C–C and B–N bond lengths were increased by 0.211% and 1.04% than their corresponding values in GRAP and BN. In addition, we also assessed the structural and thermodynamic stability of the these 2D sheets by calculating the cohesive and formation energy. The cohesive energy (E_{coh}) of all the sheets was

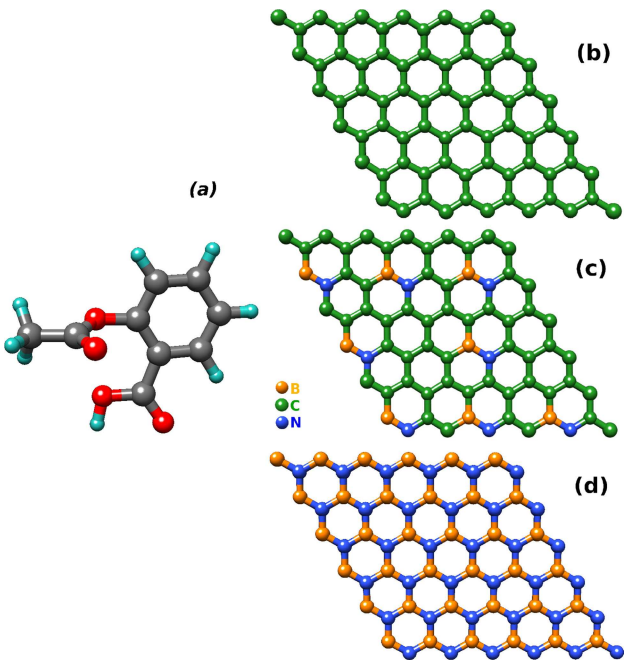

Figure 1. Optimized geometry of (a) ASA, (b,c,d) GRAP, BCN1 and h-BN sheet.

calculated using equation 2. The formation energy (E_f) was calculated for BCN sheets using equation 3. It should be noted that, in this approach the formation energy of pristine GRAP and h-BN are equal to zero, which provide us a reference value to compare the formation energy of BCN sheets with these 2D structures. For more detailed information on the calculation of cohesive and formation energy, we refer the reader to references.[34–36] The expressions used to calculate E_{coh} and E_f of GRAP, BCN and h-BN are given below.

$$E_{coh} = \left[E_{tot} - \sum_i N_i E_i\right]/N \quad (i = \mathrm{C, B, N}) \tag{2}$$

$$E_f = [E_{\mathrm{BCN}} - (n_{\mathrm{CC}}\mu_{\mathrm{CC}} + n_{\mathrm{BN}}\mu_{\mathrm{BN}})]/N \tag{3}$$

where, in equation 2, E_{tot} denotes the total energy of 2D sheet and E_i represents the gas phase atomic energies of C, B and N. N is the total number of atoms in the sheet. E_{BCN} is the total energy of BCN sheet, n_{CC} and n_{BN} denotes the CC and BN pairs in the BCN sheets and μ_{CC} and μ_{BN} corresponds to the chemical potential of C–C and B–N. The chemical potential of C–C and B–N was obtained directly from the infinite sheet energies of corresponding structures. The cohesive energies calculated for 2D sheets are given in Table 1. It is found that cohesive energy is minimum for GRAP and maximum for h-BN. While the cohesive energy of BCN (BCN1 and BCN2) sheets lies between GRAP and h-BN which demonstrates that it is less stable than GRAP but more stable than h-BN. We also calculated the formation energy of BCN sheets in order to further examine their stability. The formation energy calculated for BCN1 and BCN2 were 0.231 and 0.251 eV. Also, it is well-known that higher the cohesive and formation energy, the higher will be structural stability and greater the thermodynamic feasibility of BCN formation.[37] The chemical potential μ_{CC} and μ_{BN} obtained from graphene and h-BN sheet were −310.09 and −358.23 eV respectively which have been used in equation 3.

Table 1. The cohesive energy of GRAP, BCN1, BCN2 and h-BN, binding energy of ASA and its distance from 2D sheets.

Structure	C1		C2		
	E_{Coh}	BE	Dist	BE	Dist
GRAP	−9.138	−0.527	3.718	−0.274	5.268
BCN1	−8.812	−0.674	3.519	−0.313	5.290
BCN2	−8.780	−0.674	3.536	−0.315	5.301
h-BN	−8.711	−0.706	3.960	−0.583	5.381

The energy is in eV and distance in Å

2.2. Binding Energy of ASA

The binding energy of ASA calculated on GRAP, BCN1, BCN2 and h-BN is given in Table 1. It is important to mention that various adsorption configurations are possible when ASA molecule is adsorbed on a 2D sheet. However, it has been reported in the previous study that $\pi-\pi$ stacking configuration are the most stable configurations as compared to other stacking arrangements.[15] Therefore, in this study, we investigated two possible $\pi-\pi$ stacking configurations C1 and C2 of ASA on 2D sheets. Table 1 presents the calculated binding energy of ASA on various 2D sheets including vdW interactions which is important for adsorption calculations. It is found that magnitude of the calculated binding energy are comparatively larger in C1 as compared to C2 configuration which shows that more favorable binding of ASA occurs when oxygen atom in ester group of ASA is away from the adsorbent. We found that the binding energy of ASA is more by 0.253, 0.316 and 0.123 eV for GRAP, BCN1 and h-BN for C1 than in C2 configuration. The hierarchy of binding energy on various 2D sheets follows the order as h-BN > BCN1 = BCN2 > GRAP in C1 configuration. Moreover, the binding energy of water was calculated on various sheets and compared with that of ASA. Binding energy of water calculated on GRAP, BCN1, BCN2 and h-BN were −0.120, −0.173, −0.176 and −0.141 eV respectively. The calculated binding energy of water on different 2D substrates were found to be less that of ASA on the respective sheets. Also, in a recent study, Al-Hamdani et al.[16] calculated the binding energy of water in the range −0.089 to −0.107 ± 0.007 eV on h-BN using several theoretical methods. In another study, the interaction energy of water with GRAP was found to be in the range of −0.136 to −0.139 eV.[39] Interestingly, the binding energy of ASA on different 2D sheets considered in this study range from −0.52 to −0.70 for C1 configuration which is significantly larger than the binding energy of water on h-BN and GRAP sheet. It is worth to mention that molecular adsorption on surfaces plays an essential role in corrosion, catalysis, water purification, gas storage and many other processes that are relevant to industry.[16] From our results, it is clear that ASA strongly binds to the 2D sheets as compared to water, and hence, these 2D sheets can be used to remove aspirin molecules from waste water. The optimized structures of ASA adsorbed GRAP, BCN1 (for optimized structure of ASA on BCN2, see Figure SI4) and h-BN sheets in C1 configuration are shown in Figure 2. It is readily seen from the Figure 2 that the adsorption of ASA on h-BN sheet causes a buckling in the sheet while it does not affect the planarity of GRAP and BCN. This is due to the reason that on h-BN sheet, ASA shows strong dipole-dipole interaction with the sheet in addition of $\pi-\pi$ stacking. Similar, conclusions were drawn by Lee et al. for ASA adsorbed on carbon nitride nanotube.[15] This is also the reason for the larger binding energy of ASA with h-BN and BCN sheets as compared to graphene. Moreover, on h-BN sheet, ASA align itself in such a way that oxygen atoms of ASA lie exactly above the boron (cation) of the sheet (see Figure SI5). This shows that electron rich oxygen of ASA try to position themselves in order to maximize dipole-dipole interaction with the h-BN sheet. Examination of ASA with GRAP and BCN sheet display that ASA ring adopt AB type stacking when adsorbed on the GRAP sheet, whereas ASA ring prefers to stay on top of the carbon ring of the BCN sheet irrespective to the position of its oxygen atoms. The calculated perpendicular distance from the adsorbent to the ASA ring was 3.718, 3.519, 3.536 and 3.960 Å for GRAP,

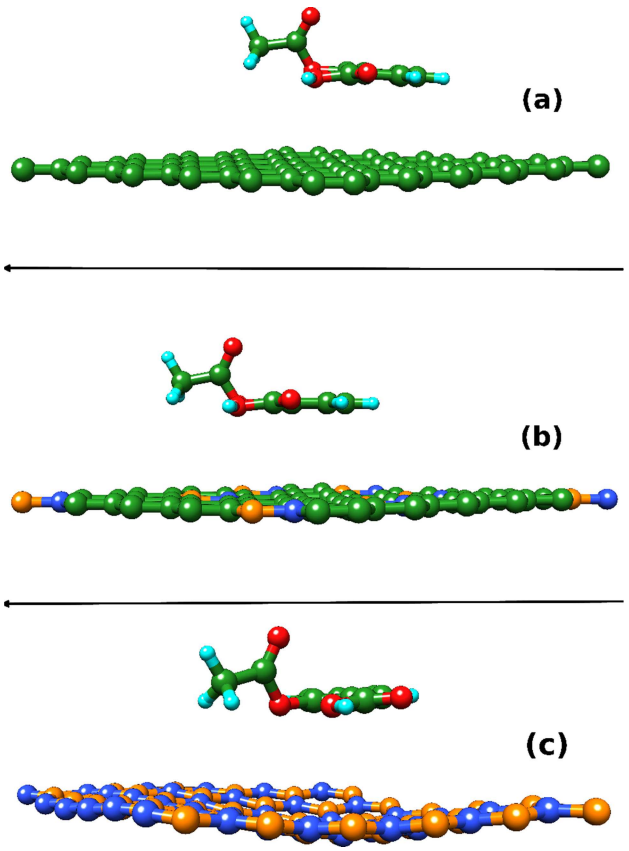

Figure 2. Side view of optimized geometry of ASA on (a) GRAP, (b) BCN1 and (c) h-BN sheet in C1 configuration.

BCN1, BCN2 and h-BN in C1 configuration as shown in Table 1. These calculated distances are larger than typical chemical bond lengths. Thus, it can be inferred that there is no charge transfer between ASA and the 2D sheets.

2.3. Electronic Structure

Electronic band structure calculations are important to see the effect of ASA on the electronic properties of pristine GRAP, BCN and h-BN. Table 2 shows the Fermi energy, valence band maximum (VBM), conduction band minimum (CBM) and band gap of pristine and ASA adsorbed GRAP, BCNand h-BN. Highest occupied molecular orbital (HOMO), lowest unoccupied molecular orbital (LUMO) energy and HOMO-LUMO gap of ASA calculated are −6.285, −2.465 and 3.820 respectively. The electronic band structure of pristine and ASA adsorbed GRAP, BCN1, BCN2 and h-BN for C1 configuration are shown in Figure 3. For C2 configuration, the corresponding band structure plots are given in SI6.

The calculated band gap of GRAP and h-BN were 0.0 and 4.319 eV respectively. Our results are consistent with the theoretical results where h-BN was found to have band gap of 4.47 eV.[32] Experimentally measured band gap of h-BN is 6.07 eV.[40] The reason that the calculated band gap is less than the experimental value is due the fact that DFT always

Table 2. Fermi energy, valence band maximum (VBM), conduction band minimum (CBM) and Band gap of pristine and ASA adsorbed GRAP, BCN and h-BN sheets.

	System	E_{Fermi}	VBM	CBM	E_{Gap}
Pristine	GRAP	−2.873	−2.878	−2.868	0.000
	BCN1	−2.802	−3.124	−2.482	0.641
	BCN2	−2.788	−3.244	−2.329	0.915
	BN	−1.428	−4.467	−0.417	4.319
	GRAP + ASA	−2.697	−2.703	−2.692	0.000
C1	BCN1 + ASA	−2.650	−2.968	−2.336	0.632
	BCN2 + ASA	−2.633	−3.097	−2.171	0.925
	h-BN + ASA	−2.684	−4.322	−1.219	3.103
	GRAP + ASA	−2.488	−2.492	−2.484	0.000
C2	BCN1 + ASA	−2.414	−2.731	−2.099	0.632
	h-BN + ASA	−2.619	−4.091	−1.206	2.885

All energies are in eV

underestimates the band gap. In addition, as can be seen from Figure 3(a), band structure of GRAP exhibits a perfect Dirac cone which arises due to the fusion of valence and conduction band at the symmetry point Γ of the Brillouin zone. For BCN sheets, we found that the band gap increases as the number of BN pairs in the GRAP sheet increases. The calculated band gaps of BCN1 and BCN2 were 0.632 and 0.926 eV respectively. Both the sheets were found to show direct band gap which is also located at high symmetry point Γ of the Brillouin zone. These results shows that ternary alloys of carbon, boron and nitrogen can have potential applications in electronics and water splitting due to their finite band gap as will be discussed in the next section. Moreover, Manna et al. have shown that by introducing BN, band gap can be opened in GRAP. In their work, the authors found that band gap of GRAP can be tuned by introducing different sized nanodomains of BN in GRAP.[37] Therefore, it can be inferred that by changing the concentration of BN in GRAP, its band gap can be tuned bearing specific application in mind. Similarly, the band gap of h-BN can be tuned by incorporating nanodomains of GRAP in the sheet. In a recent study, Ba et al. experimentally synthesized such type of sheets where they trimmed down the band gap of h-BN sheet to ≈2 eV which is about 1/3 of pristine sheet.[41]

Now, considering the influence of ASA on the band gap of GRAP, BCN, and h-BN, we found that ASA adsorbed GRAP and BCN sheet do not show any change in the band structure, as the ASA flat bands occur deep in the conduction and valence band. A negligibly small increase of 9 meV (11 meV) in the band gap was seen in ASA adsorbed BCN1 (BCN2) for C1 configuration. On the other hand, it is seen that there is a significant change in band gap of h-BN. The band gap of h-BN is reduced by 28.15% (33.20%) in configuration C1 (C2). The reduction is due to the flat band of ASA which is located at ≈1.5 eV in the band gap of h-BN. Since, we found that BCN sheets exhibit a suitable band gap and its band structure does not change upon ASA adsorption. Therefore, it can be proposed that BCN sheets can be simultaneously used for ASA adsorption and water splitting. Moreover, since ASA interacts with 2D sheets mainly through $\pi - \pi$ bonding, a clear charge transfer between ASA

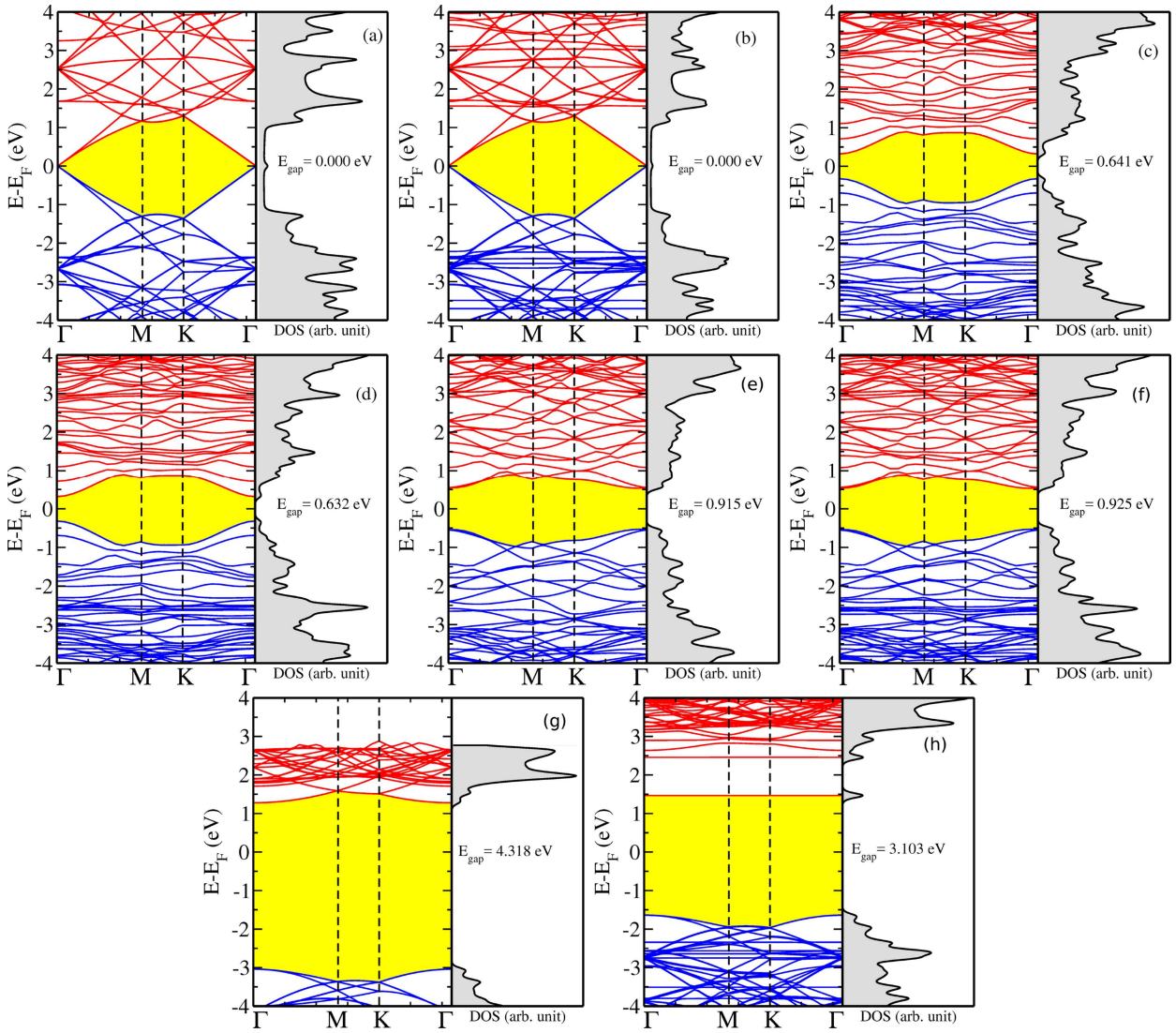

Figure 3. Band Structure of pristine and aspirin adsorption (a,b) GRAP, (c,d) BCN1, (e,f) BCN2 and (g,h) h-BN sheets in C1 configuration respectively.

and adsorbent do not occur. As a result, no molecular state of ASA contributes to the band gap edges of GRAP and BCN.

In Figure 4, we have shown the contribution of the p orbitals to the conduction and valence bands for pure and ASA adsorbed sheets. The flat bands of ASA can be clearly visualized in the projected density of states (PDOS) as shown in Figure 4. It is clear from the Figure 4 that a peak of ASA carbon is seen at 1.5 eV in the band gap of h-BN which is responsible for its band gap reduction. Another peak in the band gap is also observed at 2.5 eV. However, for GRAP and BCN1, we can see that the ASA bands lie deep in the conduction and valence band, and hence the band gap of GRAP and BCN1 sheet remains unaltered (we do not show PDOS of BCN2 as similar conclusions can be drawn for this configuration as for BCN1). In all the three cases, it is found that oxygen orbitals are located in the energy range from −2 to −3 eV in the valence band.

2.4. Hydrogen Evolution Activity

Hydrogen, a clean and environmentally benign energy source, may be produced through photocatalytic water splitting.[42,43] As we mentioned that BCN sheet may be a promising metal free candidate to simultaneously generate hydrogen and adsorb ASA due to its suitable band gap and no change in the band structure upon ASA adsorption. In addition to this, the other criteria for HER is that the band structure of the semiconductor must straddle the redox potential of water.[43] This means that the VBM must be more positive than the H_2O/O_2 level and the CBM must be more negative than the H_2O/H_2 level of water. The requirement also guarantees that without an applied bias voltage, the water-splitting reaction is energetically favourable. Therefore, the knowledge of a semiconductor's VBM and CBM positions relative to the H_2O/O_2 and the H_2O/H_2 levels respectively in water is essential for the design of a photocatalyst for water-splitting. A simple approach for this purpose

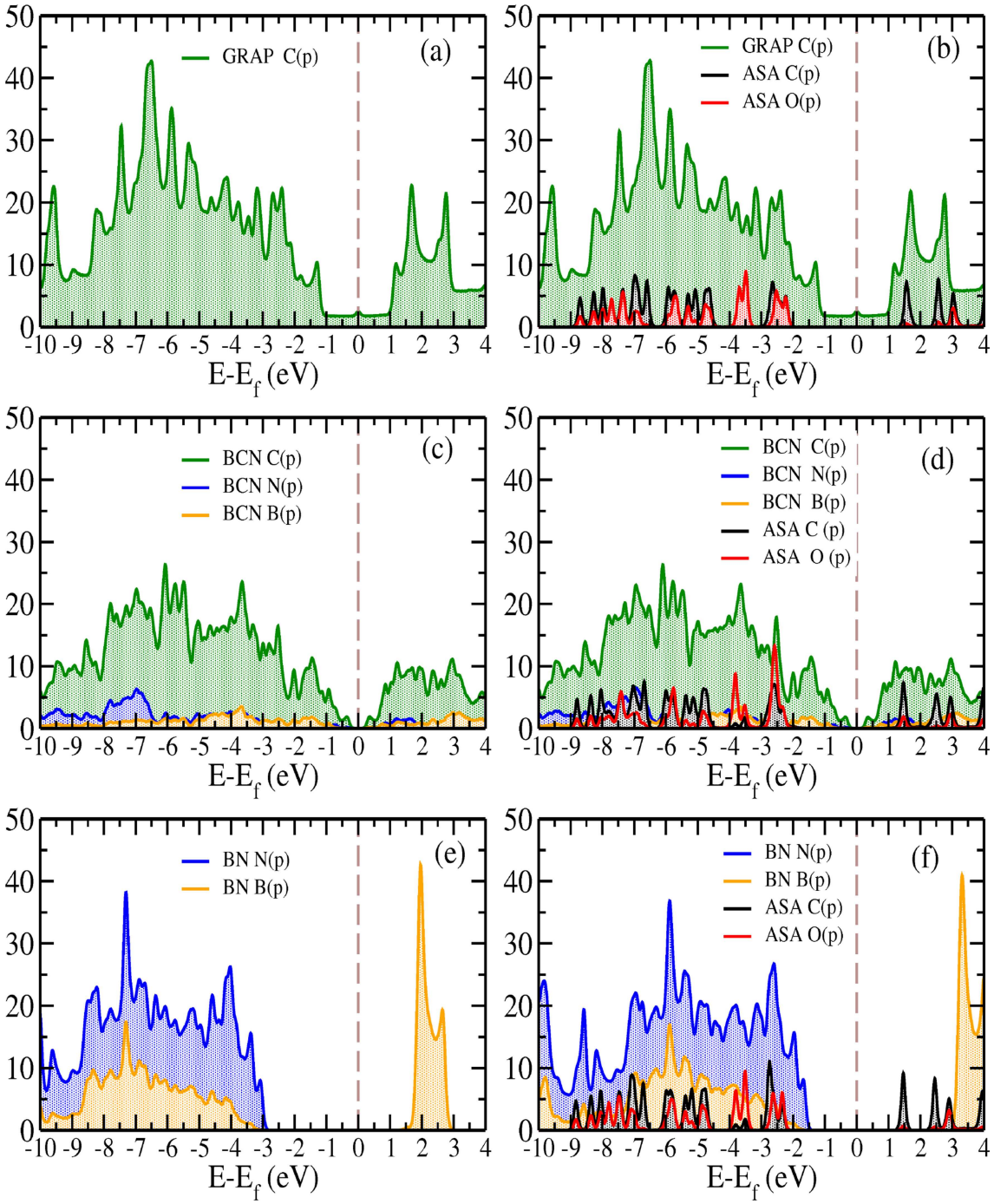

Figure 4. Projected density of states of pristine sheets and aspirin adsorbed (a,b) GRAP, (c,d) BCN1 and (e,f) h-BN sheets, respectively. In the figures, we have shown only p-orbitals.

is to compute band edge positions of a semiconductor and redox levels of water, relate them to a standard reference and then calculate their difference. And the vacuum level is a natural candidate for the standard reference level.[44] The standard redox potentials of water are −4.44 eV for reduction (H_2O/H_2) and −5.67 eV for the oxidation (H_2O/O_2) with respect to the vacuum level. As such, the band edge positions of valence and conduction bands were determined with respect to the vacuum potential of the respective sheets using the equations $E_{VBE}=E_{VBM}-E_{Vacuum}$ and $E_{CBE}=E_{CBM}-E_{Vacuum}$.

In order to prove our claim, we compared the band edge positions of pristine and ASA adsorbed BCN sheets with reducing potential of water (H_2O/H_2). Figure 5 shows the band edge positions with respect to vacuum potential of pristine and ASA adsorbed BCN sheets and HER potential of water. From the Figure 5 it is clear that the HER potential of water lies within the

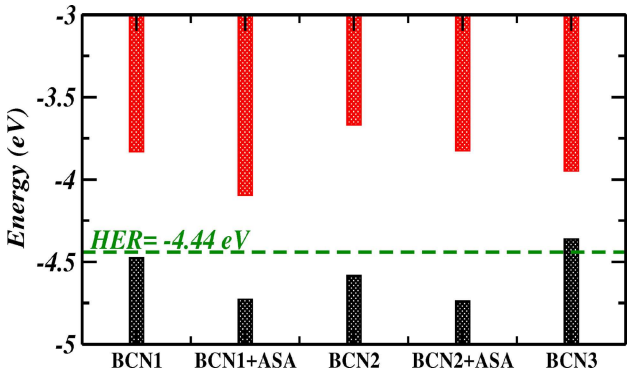

Figure 5. Energy diagram showing the conduction (red) and valance (black) band edge potentials of BCN sheets and redox potential of water.

band gap which shows that BCN sheet has the ability to reduce H_2O to H_2 and provide new opportunities in the field of photocatalysis. It is important to mention that the band gap and HER activity of BCN ternary alloys depends not only the percentage composition of C, B and N but also on the arrangement of BN pairs in the BCN sheet. To show this, we calculated the band structure of BCN3 (see Figure SI8) sheet and compared it with HER activity. The BCN3 sheet was designed in such a way as to have same concentration of C, B and N as BCN1 but with two BN pairs in one of the hexagonal rings. The calculated band gap of BCN3 sheet was 0.41 eV which is lower than BCN1 by ~0.3 eV. In addition, its conduction band edge was found to cross the HER potential. Thus, it is inferred that not only the BN concentration, but also the arrangement of BN pairs in BCN sheet affects the band gap and HER activity.

3. Conclusions

We have performed DFT calculations to investigate the structural, electronic and adsorption properties of ASA on graphene, BCN and h-BN sheets. We found that aspirin strongly binds on the sheets when oxygen atom of the ester group in ASA is away from the sheet. Binding energy of ASA on the graphene, BCN and h-BN sheets were found to be in the range of −0.52 to −0.70 eV. Also, ASA exhibits strong interaction with BCN and h-BN compared to graphene. In addition, comparing the binding energy of water and ASA on these sheets, it is concluded that all the substrates could be active candidates to remove ASA from water. From electronic band structure, we found that BCN1 and BCN2 are finite band gap semiconductors with a band gap of 0.632 and 0.923 eV and hence makes it suitable for electronic applications. Also, considering the adsorption of ASA on the various sheets, we see that no change in the band gap of graphene and BCN occurs as the ASA bands lie deep in the conduction and valence band. However, bands of ASA does occur in the band gap of h-BN which causes a reduction in its gap by 28.15% (33.20%) in configuration C1 (C2). Thus, it is concluded that BCN and h-BN can be potential candidates for detection of ASA as compared to graphene.

As a final comment, we theoretically propose that drug adsorbed BCN sheets could also be a promising candidate for HER activity. We also showed that this feature can be achieved by engineering the band gap of BN doped graphene sheet by varying the BN concentration.

Acknowledgement

V. K. Y and S. H. M gratefully acknowledge the financial support from Department of Science and Technology (grant no. SB/S3/CE/079/2015 and DST/TM/WTI/2K15/112(G)). The calculations were partly done at the High Performance Computing Facility at Computer Center, IIT Kanpur.

Conflict of Interest

The authors declare no conflict of interest.

Keywords: binding energy · borocarbonitride · density functional calculations · hydrogen evolution reaction · nanomaterials

[1] I. Villaescusa, N. Fiol, J. Poch, A. Bianchi, C. Bazzicalupi, *Desalination* **2011**, *270*, 135–142.
[2] V. Rakic, N. Rajic, A. Dakovic, A. Auroux, *Microporous Mesoporous Mater.* **2013**, *166*, 185–194.
[3] A. S. Mestre, R. A. Pires, I. Aroso, E. M. Fernandes, M. L. Pinto, R. L. Reis, M. A. Andrade, S. P. Silva, A. P. Carvalho, *Chem. Eng. J.* **2014**, *253*, 408–417.
[4] C. I. Kosma, D. A. Lambropoulou, T. A. Albanis, *Sci. Total Environ.* **2014**, *466*, 421–438.
[5] K. Mphahlele, M. S. Onyango, S. D. Mahlanga, *J. Environ. Chem. Eng.* **2015**, *3*, 2619–2630.
[6] O. C. Compton, S. T. Nguyen, *Small* **2010**, *6*, 711–723.
[7] A. C. Sophia, E. C. Lima, N. Allaudeen, S. Rajan, *Desalin. Water Treat.* **2016**, *57*, 22573–27586.
[8] C. N. R. Rao, K. Gopalakrishnan, A. Govindaraj, *Nano Today* **2014**, *9*, 324–343
[9] M. Chhetri, S. Maitra, H. Chakraborty, U. Waghmare, C. N. R. Rao, *Energy Environ. Sci.* **2016**, *9*, 95–101.
[10] K. Pramoda, M. M. Ayyub, N. K. Singh, M. Chhetri, U. Gupta, A. Soni, C. N. R. Rao, *J. Phys. Chem. C* **2017**, *122*, 13376–13384.
[11] C. N. R. Rao, K. Gopalakrishnan, *ACS Appl. Mater. Interfaces* **2016**, *9*, 19478–19494.
[12] U. A. Palnitkar, R. V. Kashid, M. A. More, D. S. Joag, L. S. Panchakarla, C. N. R. Rao, *Appl. Phys. Lett.* **2010**, *97*, 063102.
[13] R. B. Sharma, D. J. Late, D. S. Joag, A. Govindaraj, C. N. R. Rao, *Chem. Phys. Lett.* **2006**, *428*, 102–108.
[14] L. A. Al-Khateeb, S. Almotiry, M. A. Salam, *Chem. Eng. J.* **2014**, *248*, 191–199.
[15] Y. Lee, D.-G. Kwon, G. Kim, Y.-K. Kwon, *Phys. Chem. Chem. Phys.* **2017**, *19*, 8076–8081.
[16] Y. S. Al-Hamdani, *J. Chem. Phys.* **2017**, *147*, 044710.
[17] A. S. Mestre, J. Pires, J. M. F. Nogueira, J. B. Parra, A. P. Carvalho, C. O. Ania, *Bioresour. Technol.* **2009**, *100*, 1720–1726.
[18] M. Fuerhacker, A. Durauer, A. Jungbauer, *Chemosphere* **2001**, *44*, 1573–1579.
[19] P. Westerhoff, Y. Yoon, S. Snyder, E. Wert, *Environ. Sci. Technol.* **2005**, *39*, 6649–6663.
[20] A. M. Comerton, R. C. Andrews, D. M. Bagley, C. Hao, *J. Membr. Sci.* **2008**, *313*, 323–335.

[21] F Martinez, *Water Res.* **2013**, *47*, 5647–5658.
[22] Q. Dai, J. Wang, J. Yu, J. Chen, J. Chen, *Appl. Catal. B* **2014**, *144*, 686–693.
[23] Y. Yoon, P. Westerhoff, S. A. Snyder, E. C. Wert, J. Yoon, *Desalination* **2007**, *202*, 16–23.
[24] O. Lefebvre, X. Shi, C. H. Wu, H. Y. Ng, *Water Sci. Technol.* **2014**, *69*, 855–861.
[25] P. Giannozzi, S. Baroni, N. Bonini, M. Calandra, R. Car, C. Cavazzoni, D. Ceresoli, G. L. Chiarotti, M. Cococcioni, I. Dabo, *J. Phys. Condens. Matter* **2009**, *21*, 395502.
[26] D. Vanderbilt, *Phys. Rev. B* **1990**, *41*, 7892.
[27] J. P. Perdew, K. Burke, M. Ernzerhof, *Phys. Rev. Lett.* **1996**, *77*, 3865.
[28] J. P. Perdew, J. A. Chevary, S. H. Vosko, K. A. Jackson, M. R. Pederson, D. J. Singh, C. Fiolhais, *Phys. Rev. B* **1992**, *46*, 6671.
[29] A. M. Rappe, K. M. Rabe, E. Kaxiras, J. D. Joannopoulosn, *Phys. Rev. B* **1990**, *41*, 1227.
[30] H. J. Monkhorst, J. P. Pack, *Phys. Rev. B* **2005**.
[31] S. Grimme, J. Antony, S. Ehrlich, H. Krieg, *J. Chem. Phys.* **2010**, *132*, 154104.
[32] M. Topsakal, E. Akturk, S. Ciraci, *Phys. Rev. B* **2009**, *79*, 115442.
[33] J. H. Warner, G. D. Lee, K. He, A. W. Robertson, E. Yoon, A. I. Kirkland, *ACS Nano* **2004**, *7*, 205412.
[34] S. Azevedo, M. S. C. Mazzoni, R. W. Nunes, H. Chacham, *Phys. Rev. B* **2004**, *70*, 205412.
[35] S. Azevedo, *Phys. Lett. A* **2006**, *351*, 109–112.
[36] S. Azevedo, R. D. Paiva, J. R. Kaschny, *J. Phys. Condens. Matter* **2006**, *18*, 10871.
[37] A. K. Manna, S. K. Pati, *J. Phys. Chem. C* **2011**, *115*, 10842–10850.
[38] Z. E. Hughes, S. M. Tomasio, T. R. Walsh, *Nanoscale* **2014**, *6*, 5438–5448.
[39] M. Xu, T. Liang, M. Shi, H. Chen, *Chem. Rev.* **2013**, *113*, 37663798.
[40] K. Ba, W. Jiang, J. Cheng, J. Bao, N. Xuan, Y. Sun, B. Liu, A. Xie, S. Wu, Z. Sun, *Sci. Rep.* **2017**, *7*, 45584.
[41] S. H. Mir, S. Chakraborty, P. C. Jha, J. Warna, H. Soni, P. K. Jha, R. Ahuja, *Appl. Phys. Lett.* **2016**, *109*, 053903.
[42] S. H. Mir, S. Chakraborty, J. Warna, S. Narayan, P. C. Jha, P. K. Jha, R. Ahuja, *Catal. Sci. Technol.* **2017**, *7*, 687–692.
[43] Y. Wu, M. K. Y. Chan, G. Ceder, *Phys. Rev. B* **2011**, *83*, 235301.
[44] J. Kang, S. Tongay, J. Zhou, J. Li, J. Wu, *Appl. Phys. Lett.* **2013**, *102*, 012111.

Manuscript received: December 18, 2018
Accepted manuscript online: January 8, 2019
Version of record online: February 12, 2019